# MaNGA integral-field stellar kinematics of LoTSS radio galaxies: Luminous radio galaxies tend to be slow rotators

Xuechen Zheng[1], Huub Röttgering[1], Arjen van der Wel[2,3], and Michele Cappellari[4]

[1] Leiden Observatory, Leiden University, PO Box 9513, NL-2300 RA Leiden, the Netherlands
e-mail: `zheng@strw.leidenuniv.nl`
[2] Sterrenkundig Observatorium, Department of Physics and Astronomy, Ghent University, Belgium
[3] Max-Planck Institut für Astronomie, Königstuhl 17, D-69117 Heidelberg, Germany
[4] Sub-department of Astrophysics, Department of Physics, University of Oxford, Denys Wilkinson Building, Keble Road, Oxford OX1 3RH, UK

## ABSTRACT

The radio jets of an active galactic nucleus (AGN) can heat up the gas around a host galaxy and quench star formation activity. The presence of a radio jet could be related to the evolutionary path of the host galaxy and may be imprinted in the morphology and kinematics of the galaxy. In this work, we use data from the Sloan Digital Sky Survey's Mapping Nearby Galaxies at Apache Point Observatory survey and the Low Frequency Array (LOFAR) Two-Metre Sky Survey as well as the National Radio Astronomy Observatory (NRAO) the *Karl G. Jansky* Very Large Array (VLA) Sky Survey and the Faint Images of the Radio Sky at Twenty Centimeter survey. We combine these integral field spectroscopic data and radio data to study the link between stellar kinematics and radio AGNs. We find that the luminosity-weighted stellar angular momentum $\lambda_{R_e}$ is tightly related to the range of radio luminosity and the fraction of radio AGNs $F_{\text{radio}}$ present in galaxies, as high-luminosity radio AGNs are only in galaxies with a small $\lambda_{R_e}$, and the $F_{\text{radio}}$ at a fixed stellar mass decreases with $\lambda_{R_e}$. These results indicate that galaxies with stronger random stellar motions with respect to the ordered motions might be better breeding grounds for powerful radio AGNs. This would also imply that the merger events of galaxies are important in the triggering of powerful radio jets in our sample.

**Key words.** galaxies: active-galaxies:kinematics and dynamics-galaxies:jet-galaxies:supermassive black holes-radio continuum: galaxies

## 1. Introduction

A supermassive black hole (SMBH) actively accreting materials in a galaxy's centre is an active galactic nucleus (AGN). An AGN emits a large amount of energy and severely impacts the star-formation in its host galaxy (see Cattaneo et al. 2009; Fabian 2012, and reference therein). Some AGNs are bright in radio bands and have prominent jet features. These AGNs are called 'radio AGNs'. They usually reside in the centre of massive early-type galaxies (ETG; Condon & Dressel 1978; Balick & Heckman 1982; Best et al. 2005a; Brown et al. 2011). The radio jets can heat up the intergalactic materials around and therefore lower the supply of cooling gas for star-formation in their host galaxies (Best et al. 2006; Dunn & Fabian 2006; McNamara & Nulsen 2007; Fabian 2012). Although radio AGNs can be important for the evolution of galaxies, it is unclear why some galaxies contain radio AGNs and others do not. To address this radio AGN-triggering problem, we investigate links between radio AGNs and the properties of their host galaxies.

An intriguing fact about radio AGNs and their host galaxies is that the prevalence of radio AGNs is closely related to the morphology of galaxies. Barišić et al. (2019) show the fraction of radio AGNs in early-type galaxies increases with the optical axis ratio of galaxies using data from the Sloan Digital Sky Survey (SDSS; York et al. 2000; Stoughton et al. 2002), the National Radio Astronomy Observatory (NRAO) the *Karl G. Jan-*

*sky* Very Large Array (VLA) Sky Survey (NVSS; Condon et al. 2002), and the Faint Images of the Radio Sky at Twenty Centimeter survey (FIRST; Becker et al. 1995). This trend has also been confirmed for the high-luminosity radio AGNs ($L_{150\,\text{MHz}} \gtrsim 10^{23}\,\text{W\,Hz}^{-1}$) in Zheng et al. (2020) using the first data release of the LOFAR Two-metre Sky Survey (LoTSS DR1; Shimwell et al. 2019). When taking the general changes in morphology as a function of stellar mass ($M_\star$) into account in these works, the radio AGN-morphology relation cannot be explained by the trend that more massive galaxies are more likely to be round (van der Wel et al. 2009; Chang et al. 2013). The radio AGN-morphology relation probably implies that high-power radio jets preferentially exist in galaxies with a merger-dominant history, which are more likely to be round. This interpretation is in line with the results from the decomposition of the optical light profile of radio galaxies (Wang et al. 2016, 2019) and deep imaging (Tadhunter 2016; Pierce et al. 2019), where the host galaxies of high-luminosity radio AGNs show more post-merger features than their low-luminosity counterparts.

We note that the link between radio AGNs and galaxy morphology is luminosity dependent. Zheng et al. (2020) indicated that the fraction of galaxies hosting low-luminosity ($L_{150\,\text{MHz}} \lesssim 10^{23}\,\text{W\,Hz}^{-1}$) radio AGNs does not depend on the axis ratio of galaxies. A large fraction of low-luminosity radio AGNs show no morphological signs of merging events and have disc-like components in optical images (e.g. Wang et al. 2019; Pierce et al. 2019). Therefore, it has been suggested that high- and low-luminosity radio AGNs may be triggered in different ways.

The radio luminosity-morphology relation may be explained by the spin paradigm (Blandford & Znajek 1977; Wilson & Colbert 1995; Sikora et al. 2007; Fanidakis et al. 2011; Chen et al. 2021). As described in Blandford & Znajek (1977), the spin of an SMBH is an essential ingredient in the jet-launching process. Numerical simulations have shown that both accretion processes and black hole mergers can change the spin of SMBHs (Fanidakis et al. 2011; Dubois et al. 2014; Bustamante & Springel 2019). The black hole merger was believed to be an efficient way to make a high-spin SMBH (Wilson & Colbert 1995; Sikora et al. 2007; Fanidakis et al. 2011) and led to the conclusion that merged SMBHs are more likely to launch radio jets. Although this hypothesis has been challenged by both observational and numerical works (Garofalo et al. 2010; Reynolds 2013; Dubois et al. 2014; Bustamante & Springel 2019; Sayeb et al. 2021, see Section 4 for more discussion), it is still reasonable to suggest that SMBHs in galaxies without mergers in their evolution path would have different spins than those in galaxies with a merger-driven history because the merging of galaxies would be followed by the merging of SMBHs.

When deep images are not available, it is difficult to verify whether a galaxy has a merger-dominant history with traditional imaging because of projection effects. Integral field spectroscopic (IFS) observation, which can resolve the stellar velocity field in galaxies, presents a good way of overcoming this difficulty. The pioneering work of Smith et al. (1990) has shown that the stellar dynamics of galaxies can indeed provide valuable clues for studying the triggering of powerful radio AGNs. Recently, IFS surveys such as the ATLAS³D survey (Cappellari et al. 2011a), the Calar Alto Legacy Integral Field Area survey (Sánchez et al. 2012), and the Mapping Nearby Galaxies at APO (MaNGA; Bundy et al. 2015) survey have greatly improved our understanding about the structure and stellar kinematics of galaxies. These surveys have shown that ETGs can be separated into two categories, fast rotators (FRs) and slow rotators (SRs), based on stellar kinematics (see Cappellari 2016, and reference therein). The FRs have disc-like structures and rotation-dominated kinematics, while the SRs have no disc and random motion dominated kinematics. The structure and stellar kinematics of these galaxies indicate their evolutionary paths. Because disc structure can be easily preserved or rebuilt in gas-rich processes, such as gas accretion and wet mergers, SRs are most likely the products of major dry mergers, after which the stellar discs are disrupted and not enough gas is available to rebuild them. (Bender et al. 1992; Emsellem et al. 2011; Bois et al. 2011; Lauer 2012; Cappellari 2016).

The FR-SR dichotomy seems to directly relate to the morphological difference in high- and low-luminosity radio AGNs. In this work, we combine the observational results from MaNGA and LoTSS to investigate the stellar kinematics of high- and low-luminosity radio AGNs. This can help verify the link between radio jets and a galaxy's evolution path. This article is organised as follows: We describe our sample in Section 2. The analyses and results are shown in Section 3. In Section 4, we summarise the main findings of this work. The cosmology adopted throughout the work is $H_0 = 70\,\mathrm{km\,s^{-1}\,Mpc^{-1}}$, $\Omega_M = 0.3$, $\Omega_\Gamma = 0.7$.

## 2. Data and sample

The IFS data in this work are from the MaNGA Data Release 16 (DR16; Ahumada et al. 2020). The MaNGA survey uses the intergral field units (IFUs) equipped by the Baryon Oscillation Spectroscopic Survey (BOSS) spectrographs on the 2.5-metre Sloan Telescope (Smee et al. 2013). These IFUs have 19

to 127 hexagonally bundled 2" fibres corresponding to diameters of 12" to 32". The final spectra provided by the MaNGA covers wavelengths from 360 to 1000 nm, with a resolution of $R \sim 2000$ (Law et al. 2016). The MaNGA DR16 contains a total of 4597 galaxies from an extended version of the NASA-Sloan Atlas (NSA[1]). These galaxies are selected to have a flat number density distribution in the *i*-band absolute magnitude within $0.01 < z < 0.15$ (Wake et al. 2017). This selection strategy ensures that the galaxy sample has a flat stellar mass distribution between $10^9 - 10^{12} M_\odot$. Galaxies in the primary and secondary samples of MaNGA are mapped by IFUs out to 1.5 and 2.5 effective radii ($R_e$), respectively.

The kinematic and morphological parameters of the MaNGA galaxies were measured by Graham et al. (2019) (hereafter 'G19') and tabulated in Bevacqua et al. (2022). These galaxies were flagged based on the criteria in Graham et al. (2018) to exclude problematic data, merging sources that have hard to define morphological parameters and sources too small with respect to the point spreading function of the Sloan Telescope. After the exclusion of these sources, the rest of the galaxies formed the 'clean' sample, as defined in G19, which comprises 4003 sources. These galaxies all have reliable kinematic and morphological measurements. The galaxies used in our analysis are all from the clean sample.

To study the stellar kinematics of the galaxies, G19 measured the luminosity-weighted stellar angular momentum within one $R_e$ ($\lambda_{R_e}$), defined in Emsellem et al. (2007),

$$\lambda_{R_e} = \frac{\sum_{n=1}^{N} F_n R_n |V_n|}{\sum_{n=1}^{N} F_n R_n \sqrt{V_n^2 + \sigma_n^2}},\tag{1}$$

where $F_n$, $R_n$, $V_n$, and $\sigma_n$ are respectively the flux, projected radius, projected stellar velocity, and velocity dispersion of the *n*-th spatial bin. The typical error of $\lambda_{R_e}$ in the catalogue is less than 0.05 (Graham et al. 2018). The galaxies with ellipticity $\epsilon < 0.4$ and $\lambda_{R_e} < 0.08 + \epsilon/4$ were classified as SRs, while the others were classified as FRs (Emsellem et al. 2011; Cappellari 2016; Graham et al. 2018).

To identify the radio AGNs in the MaNGA sample, we used the data from the LoTSS Data release two (DR2; Shimwell et al. 2019). The LoTSS DR2 covers 27% of the northern sky at 120–169MHz. This survey achieves a median sensitivity of $83\,\mu$Jy beam$^{-1}$ and an astrometric accuracy of 0.2" at 6" resolution for bright sources. A total of 4396228 radio sources were detected in LoTSS DR2. Because of the high sensitivity and the large sky coverage, LoTSS DR2 is expected to have many low-luminosity radio AGNs, which makes it a good dataset for our work.

We used the cross-matching results from Mulcahey et al. (2022), hereafter 'M22', to classify the radio AGNs in the MaNGA sample. M22 used a 5"-matching radius to match the positions in the source catalogues of the MaNGA and LoTSS DR2. This matching resulted in a radio sample of 1410 MaNGA sources with a false positive rate of less than 10%. At low luminosity, the contribution of star-forming galaxies in a radio source sample becomes important (Best & Heckman 2012; Sabater et al. 2019). Therefore, M22 separated these radio sources into radio AGNs and star-forming galaxies based on four diagnostics: the $D_n4000 - L_{150\,\mathrm{MHz}}/M_*$ diagram; the [NII] Baldwin, Phillips, and Telervich (BPT; Baldwin et al. 1981) diagram; $L_{H\alpha} - L_{150\,\mathrm{MHz}}$; and the colour from the Wide-Field Infrared Survey Explorer (WISE; Wright et al. 2010). This classification

---

[1] http://www.nsatlas.org
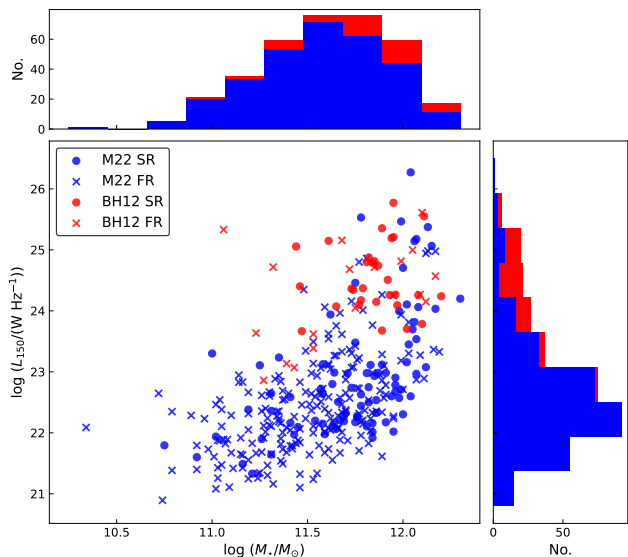
**Fig. 1.** Radio luminosity and stellar mass distributions of the final radio AGN sample in this work. The blue data points and histograms represent the 300 radio AGNs from the M22 sample based on LoTSS DR2. The red data points and bars stacked on the blue histograms denote the other 49 radio AGNs identified in Best & Heckman (2012). We use circles and crosses to mark the SRs and FRs, respectively, classified by Graham et al. (2019).

| $\log(M_\star/M_\odot)$ | 11.2–11.5 | 11.5–11.8 | >11.8 |
|---|---|---|---|
| LoTSS AGN | 70 | 106 | 78 |
| BH12 AGN | 8 | 12 | 28 |
| Total AGN | 78 | 118 | 106 |
| Galaxy | 575 | 468 | 286 |

**Table 1.** Number of sources in the three $M_\star$ bins in Section 3.1. The number of AGNs from the LoTSS DR2 and BH12 are listed separately. The number of galaxies is based on the G19's clean galaxy sample in the FoVs of either LoTSS DR2 or SDSS DR7.

$L_{150\,\mathrm{MHz}} = 10^{21} - 10^{24}\,\mathrm{W\,Hz^{-1}}$. Over 86% of these radio AGNs are hosted by passive galaxies based on the colour-colour criteria in Chang et al. (2015) ($u-r > 1.6\times(r-z)+1.1$). Nearly all the radio AGNs identified in BH12 are above $L_{150\,\mathrm{MHz}} = 10^{23}\,\mathrm{W\,Hz^{-1}}$ and therefore complement the LoTSS DR2 sample, which has only a very small number of sources at high luminosity, and improve the coverage of the $L_{150\,\mathrm{MHz}}$ -$z$ plane for the more luminous sources. The rotator type of each source is also marked in Figure 1. No significant trend between the rotator type and radio luminosity was found.
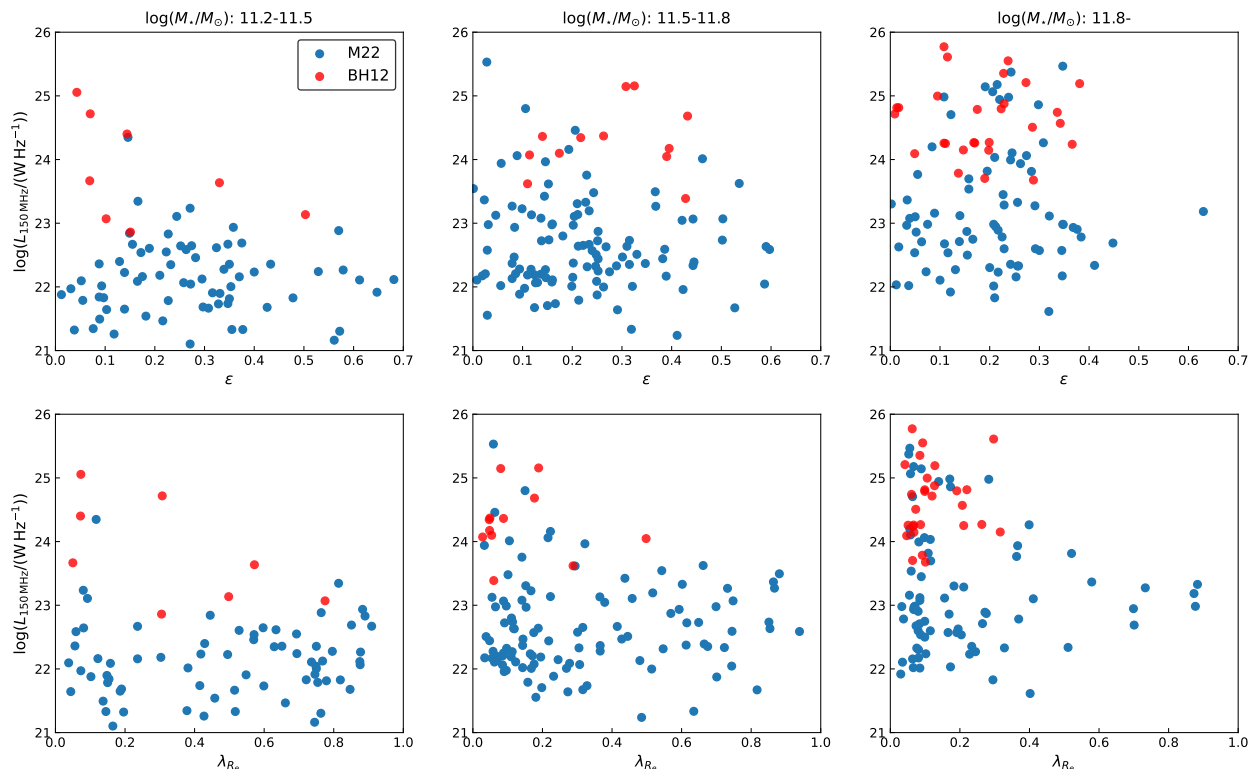
## 3. Data analysis

### 3.1. The $\epsilon$ and $\lambda_{R_e}$ of galaxies hosting a radio AGN

Previous studies have found that the radio luminosity distribution of radio AGNs is linked with the optical projected axis ratio $q$ (the ratio of the minor axis to the major axis; Zheng et al. 2020, 2022). Galaxies with a large $q$ (>0.6) can host a high-power radio AGN with $L_{150\,\mathrm{MHz}} \gtrsim 10^{23.5}\,\mathrm{W\,Hz^{-1}}$, while galaxies with a small $q$ host radio AGNs mostly with a lower radio luminosity. This trend can be seen in the radio AGNs' distribution on the $L_{150\,\mathrm{MHz}}$ -$q$ plane, where most radio AGNs are distributed in a triangle area and leave the small-$q$-high-$L_{150\,\mathrm{MHz}}$ region empty (see Figure 3 in Zheng et al. 2020).

The radio AGNs in this work should follow the $L_{150\,\mathrm{MHz}}$ -$q$ distribution found in previous works. We selected radio AGNs from three $M_\star$ bins with a high number of sources: $\log(M_\star/M_\odot)$ = 11.2 − 11.5, 11.5 − 11.8, and > 11.8. The total number of radio AGNs and galaxies within the $M_\star$ ranges is 302 and 1379, respectively. The number of sources in each of these three bins is listed in Table 1. Because $M_\star$ is correlated to both the radio luminosity and the morphology of galaxies (Chang et al. 2013; Sabater et al. 2019), constraining the $M_\star$ range is necessary to show a pure luminosity-morphology correlation. In the catalogue from G19, the $\epsilon$ of galaxies was provided and can be written as $\epsilon = 1 - q$. The resulting distributions of radio AGNs in the $L_{150\,\mathrm{MHz}}$ -$\epsilon$ plane in the three $M_\star$ bins are shown in the upper panels of Figure 2.

In the first $M_\star$ bin, while 13 of the 72 radio AGNs with $L_{150\,\mathrm{MHz}} < 10^{23.5}\,\mathrm{W\,Hz^{-1}}$ have a large ellipticity $\epsilon > 0.4$, none of radio AGNs with higher luminosity have a large ellipticity. This means that a high-power radio AGN is not likely to reside in an elongated galaxy, which is in line with previous studies (Barišić et al. 2019; Zheng et al. 2020). We note that this difference between high- and low-power radio AGNs does not seem to be significant in higher $M_\star$ bins. This is mainly because most of the massive galaxies are round elliptical galaxies with a small $\epsilon$. In our sample, more than 90% of the galaxies with $M_\star > 10^{11.8}\,M_\odot$ have an $\epsilon$ smaller than 0.4.

The apparent ellipticity of galaxies can greatly differ from the intrinsic ellipticity because of projection effects (Binney 1985). Therefore, the observed $\epsilon$ is not an ideal proxy for the

process was performed for LoTSS DR1, and the contamination rate from star-forming galaxies was estimated to be less than 3% (Sabater et al. 2019). Combining the results from M22 and G19, we obtained a clean MaNGA-radio AGN sample that consists of 300 radio AGNs with reliable stellar kinematic measurements. We also obtained a total of 2796 galaxies in G19's clean sample that fall into the field of view (FoV) of the LoTSS DR2.

We note that the simple cross-matching process may miss some luminous radio AGNs that can have a large angular size in the sky. Moreover, some MaNGA sources are outside the FoV of LoTSS DR2. Therefore, we also matched the MaNGA sample with the radio sources catalogue provided in Best & Heckman (2012), hereafter 'BH12', which is based on the NVSS-FIRST data and the SDSS data release 7 (DR7; Abazajian et al. 2009). This added 1090 galaxies covered by the FoV of SDSS DR7 from G19's clean sample. The radio catalogue from BH12 used a more careful hybrid cross-matching method in the identification of optical counterparts (Best et al. 2005b; Donoso et al. 2009). This dataset has a radio flux limit of 5 mJy and mainly contains radio sources with $L_{1.4\,\mathrm{GHz}} > 10^{23}\,\mathrm{W\,Hz^{-1}}$. The radio AGNs in this catalogue and in M22 are classified in a similar way (see Appendix 1 in BH12). In this way, we obtained 49 more radio AGNs with kinematic measurements. Therefore, our final sample contains 3886 galaxies, of which 349 are radio AGNs.

The radio luminosity and stellar mass distributions of our final radio AGN sample are shown in Figure 1. The stellar masses used in this work are taken from the source catalogue of Graham et al. (2019), which is based on the calibration of the dynamical mass against the K-band luminosity of Cappellari (2013). The radio luminosities were determined using the redshifts taken from NSA and a canonical radio spectral index of 0.7. The majority of the radio AGNs are within $M_\star = 10^{11} - 10^{12.5}\,M_\odot$ and

**Fig. 2.** $L_{150\,\mathrm{MHz}}$ of radio AGNs versus the $\epsilon$ and $\lambda_{R_e}$ of their host galaxies. The top panels show the $L_{150\,\mathrm{MHz}}$ of radio AGNs as a function of the $\epsilon$ of the host galaxies in three $M_\star$ bins (from left to right): $\log(M_\star/M_\odot) = 11.2 - 11.5$, $11.5 - 1.8$, and $> 11.8$. The bottom panels show the $L_{150\,\mathrm{MHz}}$ as a function of the $\lambda_{R_e}$ of the host galaxies in three $M_\star$ bins. In all panels, the blue points denote radio AGNs from M22, and the red points denote radio AGNs from the BH12 sample.

kinematics of galaxies. To better describe the kinematic features of galaxies, we use $\lambda_{R_e}$, which quantifies the importance of the regular motions with respect to the random motion of stars in galaxies by definition.

We plotted the radio AGNs in the three $M_\star$ bins on the $L_{150\,\mathrm{MHz}}$-$\lambda_{R_e}$ plane, shown in the bottom panels of Figure 2. The distribution of the radio AGNs is clearly characterised by a triangle zone with nearly no radio AGNs appearing in the large-$\lambda_{R_e}$-high-$L_{150\,\mathrm{MHz}}$ area. The maximum $L_{150\,\mathrm{MHz}}$ of radio AGNs decreases dramatically with $\lambda_{R_e}$ in all three $M_\star$ bins. In the first $M_\star$ bin, the fraction of large $\lambda_{R_e}(\lambda_{R_e}>0.4)$ sources is 0/4 for radio AGNs with $L_{150\,\mathrm{MHz}} > 10^{24}\,\mathrm{W\,Hz}^{-1}$ and 47/74 for those with lower luminosity. These fractions become 1/15 versus 35/102 in the second bin and 0/41 versus 11/65 in the third bin. This result indicates that the radio AGNs with $L_{150\,\mathrm{MHz}} > 10^{24}\,\mathrm{W\,Hz}^{-1}$ in our sample are triggered in galaxies with $\lambda_{R_e} \lesssim 0.4$. Furthermore, the comparison between the $L_{150\,\mathrm{MHz}}$-$\epsilon$ and $L_{150\,\mathrm{MHz}}$-$\lambda_{R_e}$ diagrams implies that the $L_{150\,\mathrm{MHz}}$-$\lambda_{R_e}$ relation is a powerful tool for studying the intrinsic relations between radio AGNs and the kinematics of their host galaxies.

In summary, we show the location of the radio AGNs in the $\epsilon$-$\lambda_{R_e}$ plane in Figure 3. Apparently, luminous radio AGNs tend to be in SRs, which have both a small $\epsilon$ and $\lambda_{R_e}$. On the contrary, less luminous radio AGNs can be found in many FRs. The

fractions of SRs in high-power AGNs are $50^{+22}_{-22}\%$,[2] $56.3^{+11.7}_{-12.4}\%$, and $68.3^{+6.8}_{-7.6}\%$ in the three bins, while the fractions in low-power AGNs are $16.2^{+4.8}_{-3.9}\%$, $24.5^{+4.5}_{-4.0}\%$, and $53.8^{+6.1}_{-6.2}\%$. In all three bins, high-power radio AGNs have a significantly higher fraction of SRs in contrast to low-power radio AGNs. Because SRs have been argued to have a dry-merger dominant history, in contrast to FRs, we suggest that the difference in the $\epsilon$-$\lambda_{R_e}$ distributions of high- and low-luminosity radio AGNs at fixed $M_\star$ stems from the different evolutionary paths of the host galaxies.

### 3.2. Prevalence of radio AGNs

When inspecting the distributions of galaxies and radio AGNs in the $\epsilon$-$\lambda_{R_e}$ plane in Figure 3, we found that more massive galaxies have a higher fraction of radio AGNs and have a higher radio luminosity. This is in line with previous studies based on large radio surveys (e.g. Best et al. 2005a; Sabater et al. 2019) that showed that the fraction of galaxies hosting a radio AGN, $F_{\mathrm{radio}}$, is tightly related to stellar mass and radio luminosity. Figure 3 also shows that the fraction of high-luminosity radio AGNs seems to decrease with either $\lambda_{R_e}$ or $\epsilon$, which is consistent with the correlations between $F_{\mathrm{radio}}$ and the shape of galaxies in Barišić et al. (2019) and Zheng et al. (2020). In this section, we

---

[2] The errors of these fractions show the $1\sigma$ Agresti-Coull confidence limits(Agresti & Coull 1998).
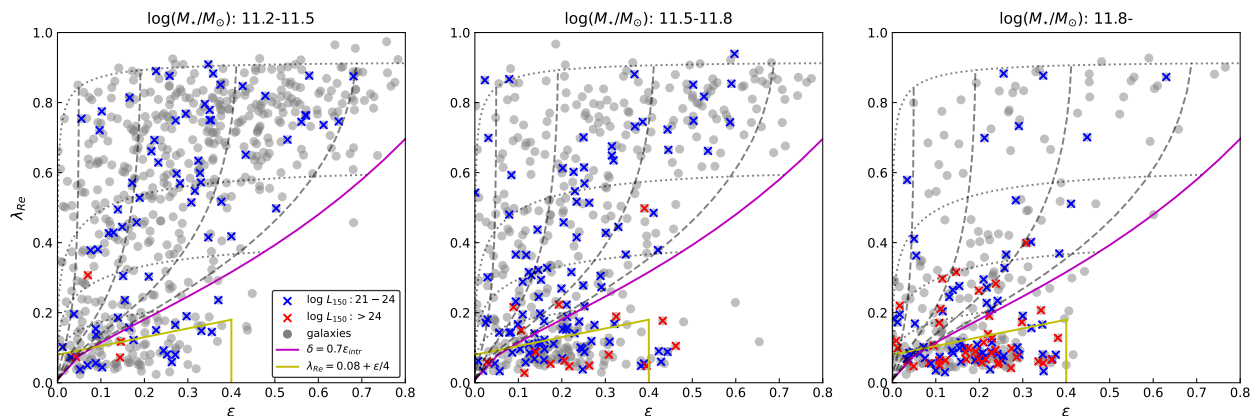
**Fig. 3.** Distributions of galaxies and radio AGN in the $\epsilon$-$\lambda_{R_e}$ plane. From left to right, the three panels show the distributions of galaxies in three $M_\star$ bins: $\log(M_\star/M_\odot)$=11.2 − 11.5, 11.5 − 1.8, and > 11.8. The total number of AGNs and galaxies within these $M_\star$ ranges are 302 and 1329, respectively. The source number in each $M_\star$ bin is listed in Table 1. The blue and red crosses mark the radio AGNs with $\log(L_{150 MHz})$=21 − 24 and > 24, and the grey points denote the galaxies within the corresponding $M_\star$ bin. The yellow lines denote the separation of SRs and FRs proposed by Cappellari (2016). The magenta line shows the estimated $\lambda_{R_e}$ of edge-on FR galaxies with maximum anisotropy $\delta = 0.7\epsilon_{intr}$ described in Cappellari et al. (2007), where $\epsilon_{intri}$ denotes the intrinsic ellipticity. The grey dashed and dotted lines show the $\lambda_{R_e}$ for FRs with different inclinations and $\epsilon_{intr}$, respectively.

investigate these trends with a focus on how the kinematics of galaxies may influence $F_{radio}$.

We define $F_{radio}$ as

$$F_{radio}(\theta_1, \theta_2, ...) = \frac{N_{radioAGN}(\theta_1, \theta_2, ...)}{N_{galaxy}(\theta_1, \theta_2, ...)}, \qquad (2)$$

where $N_{radioAGN}$ is the number of radio AGNs identified in either the M22 or BH12 sample, $N_{galaxy}$ is the number of galaxies covered by the FoV of the LoTSS DR2 or the SDSS DR7, and $\theta_i$ denotes an arbitrary parameter constraint in the source selection (e.g. $M_\star$, $L_{150 MHz}$, $\lambda_{R_e}$). We note that our $F_{radio}$ results should only be taken as an accurate measurement for the prevalence of radio AGNs if the sensitivity variation across the FoV and the change in the detectability of certain galaxies at different redshifts are considered in the calculation. As we do not do so, our results may differ from those of previous works (Best et al. 2005a; Sabater et al. 2019). However, in this work we focus on the relative change of $F_{radio}$ in galaxies with different kinematics, and this change should not be influenced by these factors. Our simple estimation of $F_{radio}$ should be adequate for the goals in this paper.

We first divided the sources into two groups with different $\epsilon$ and compared the $F_{radio}$ -$M_\star$ relations within the two groups. We choose $\epsilon = 0.3$ as the division line because it is roughly where the radio luminosity distribution changes, as shown in Figure 2. This $\epsilon = 0.3$ division also ensures the group with a larger $\epsilon$ has enough sources for the $F_{radio}$ calculations. We calculated the $F_{radio}$ in five logarithmic, equidistant $M_\star$ bins between $10^{10.5}$ to $10^{12.5}$ $M_\odot$. The results are shown in the top-left panel of Figure 4. The error bars are the $1\sigma$ Agresti-Coull confidence limit (Agresti & Coull 1998). To investigate how the radio AGN-morphology relation changes with radio luminosity, we further calculated the $F_{radio}$ for low- and high-luminosity radio AGNs with $L_{150 MHz}$ lower and higher than $10^{23.5}$ W Hz$^{-1}$ and show the $F_{radio}$ in the top-middle and top-right panels of Figure 4.

The $F_{radio}$ for all radio AGNs in both the large- and small-$\epsilon$ groups follow the canonical increasing trend with $M_\star$ (Best et al. 2005b; Sabater et al. 2019). The $F_{radio}$ of the large-$\epsilon$ galaxies are slightly smaller than those of the small-$\epsilon$ galaxies in most bins.

However, these differences do not seem to be significant, as they are typically within the $1\sigma$ error bars. This result is in line with the findings in Zheng et al. (2020), where the $F_{radio}$ of oblate galaxies are close to the $F_{radio}$ of triaxial galaxies. The marginal differences between the $F_{radio}$ of large- and small-$\epsilon$ galaxies are also present in the results for high- and low-luminosity radio AGNs. Although in the most massive bin the large-$\epsilon$ galaxies have a higher $F_{radio}$ for high-luminosity radio AGNs, the number of sources in the bin is too small for this result to be significant.

We then separated the sources into two groups based on the $\lambda_{R_e}$ to investigate the $F_{radio}$ -$M_\star$ relation for galaxies with different kinematics. We chose $\lambda_{R_e}$ = 0.2 as the dividing line based on the $L_{150 MHz}$ -$\lambda_{R_e}$ distribution in Figure 2. The $F_{radio}$ results are shown in the middle row of Figure 4.

Based on Figure 4, it is apparent that the low-$\lambda_{R_e}$ galaxies have a significantly higher $F_{radio}$ than the high-$\lambda_{R_e}$ galaxies in almost all $M_\star$ bins with reliable $F_{radio}$ results (small error bars). Moreover, this trend does not change for radio AGNs with different radio luminosities. This result shows that both low- and high-luminosity radio AGNs are more likely to be triggered in galaxies with a low-$\lambda_{R_e}$.

Finally, we also separated the sources based on their rotator type in G19. We show the results in the bottom row of Figure 4. The results are largely similar to those of the $\lambda_{R_e}$ groups. This is because the SRs are all low-$\lambda_{R_e}$ galaxies by definition.

To understand in more detail the $F_{radio}$ dependence on galaxy morphology and kinematics, we also calculated the $F_{radio}$ as a function of either $\epsilon$ or $\lambda_{R_e}$. We chose galaxies with $M_\star$ values ranging from $10^{11}$ to $10^{12}$ $M_\odot$ where the sample has a large source number and shows the largest difference in $F_{radio}$ for galaxies with different $\epsilon$ or $\lambda_{R_e}$ in Figure 4. To enlarge the source number in each bin and reduce the error bars of the $F_{radio}$, we split the sources into two $M_\star$ groups, one with $\log(M_\star/M_\odot)$=11−11.5 and another with 11.5−12, and we calculated the $F_{radio}$ in five equidistant $\epsilon$ or $\lambda_{R_e}$ bins. We only included sources with $\epsilon = 0 − 0.8$ and $\lambda_{R_e} = 0 − 0.9$ because the number of sources with large $\epsilon$ and $\lambda_{R_e}$ is very low. The number of AGNs in these two groups is 108 and 186, respectively, and the num-
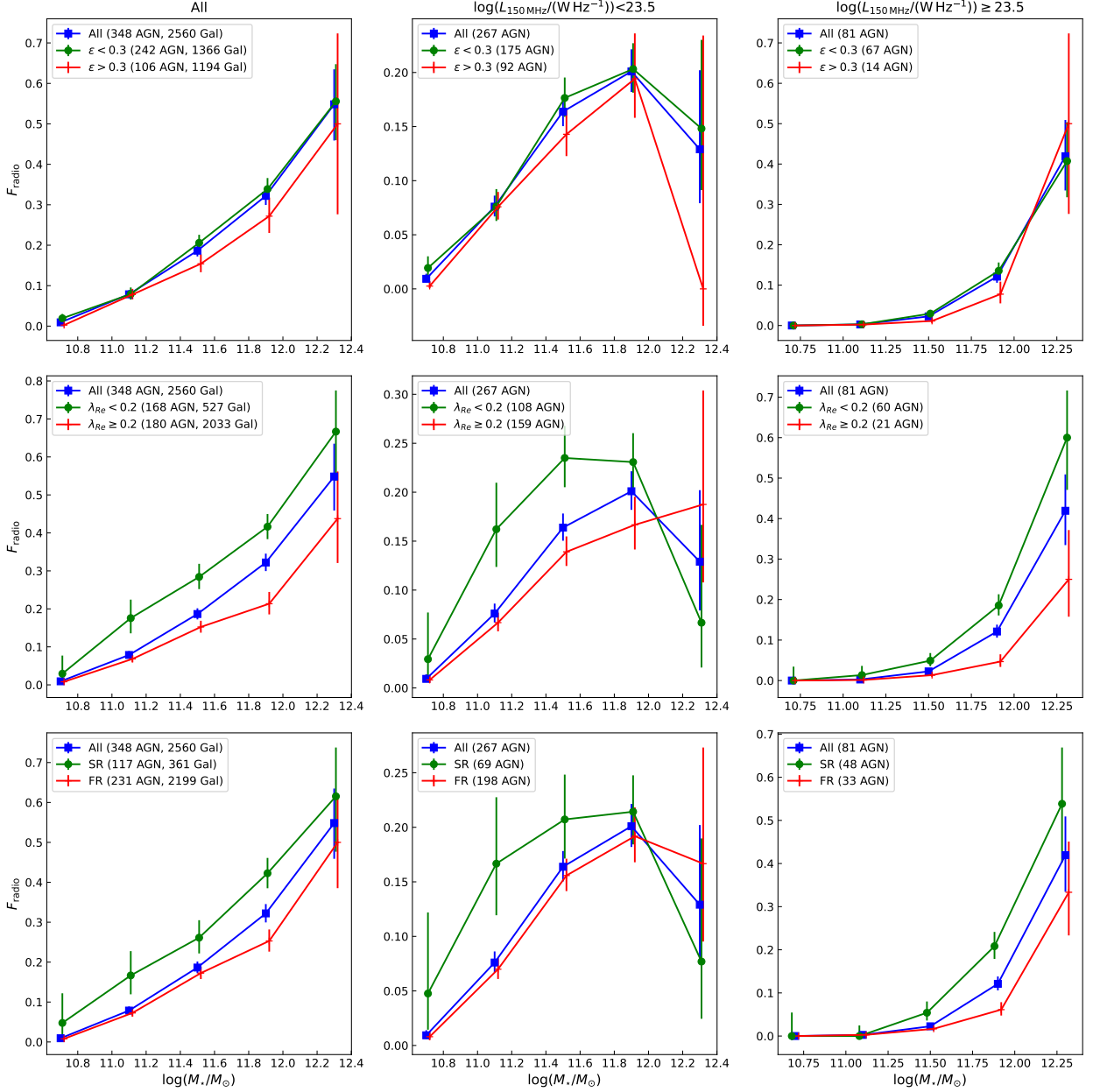
**Fig. 4.** $F_{\mathrm{radio}}$ -$M_{\star}$ relations in different galaxies. From left to right, the three panels in each row show the $F_{\mathrm{radio}}$ for all radio AGNs, radio AGNs with $L_{150\,\mathrm{MHz}} < 10^{23.5}\,\mathrm{W\,Hz^{-1}}$, and radio AGNs with $L_{150\,\mathrm{MHz}} \geq 10^{23.5}\,\mathrm{W\,Hz^{-1}}$. Top row: $F_{\mathrm{radio}}$ -$M_{\star}$ relations for galaxies with different $\epsilon$. The blue squares denote the $F_{\mathrm{radio}}$ for all galaxies, and the green points and red dots denote the $F_{\mathrm{radio}}$ for galaxies with $\epsilon < 0.3$ and $\epsilon > 0.3$, respectively. The three lines were shifted a bit horizontally for clarity. Middle row: $F_{\mathrm{radio}}$ -$M_{\star}$ relations for galaxies with different $\lambda_{R_e}$. The blue squares denote the $F_{\mathrm{radio}}$ for all galaxies, and the green points and red dots denote the $F_{\mathrm{radio}}$ for galaxies with $\lambda_{R_e} < 0.2$ and $\lambda_{R_e} > 0.2$, respectively. Bottom row: $F_{\mathrm{radio}}$ -$M_{\star}$ relations for galaxies with different rotator types. The blue squares denote the $F_{\mathrm{radio}}$ for all galaxies, and the green points and red dots denote the $F_{\mathrm{radio}}$ for SRs and FRs, respectively. The number of AGNs used in each $F_{\mathrm{radio}}$ relation is listed in the corresponding panel. The number of galaxies used in the $F_{\mathrm{radio}}$ calculations is listed in the left panel of each row, and the $F_{\mathrm{radio}}$ in the middle and right panels was calculated based on the same galaxy sample as in the left panels. All error bars are the $1\sigma$ Agresti-Coull confidence limits (Agresti & Coull 1998).

ber of galaxies is 902 and 667, respectively. The $F_{\mathrm{radio}}$ results are shown in the top panels of Figure 5.

For the $F_{\mathrm{radio}}$ -$\epsilon$ relation, the $F_{\mathrm{radio}}$ shows a weak decreasing trend in the low-$M_{\star}$ group. In the high-$M_{\star}$ groups, the $F_{\mathrm{radio}}$ does not change until $\epsilon = 0.4$, where it then drops dramatically. This may explain the marginal differences in the $F_{\mathrm{radio}}$ for

the large- and small-$\epsilon$ galaxies in Figure 4, where a division line of $\epsilon = 0.3$ was adopted. We note that the $F_{\mathrm{radio}}$ -$\epsilon$ relation for the high-$M_{\star}$ galaxies is not directly in line with the $F_{\mathrm{radio}}$ -$q$ relations in Barišić et al. (2019) or Zheng et al. (2020), as the $F_{\mathrm{radio}}$ -$q$ relation in Barišić et al. (2019) did not have a plateau and the $F_{\mathrm{radio}}$ was not dependent on $q$ in Zheng et al. (2020). A likely rea-
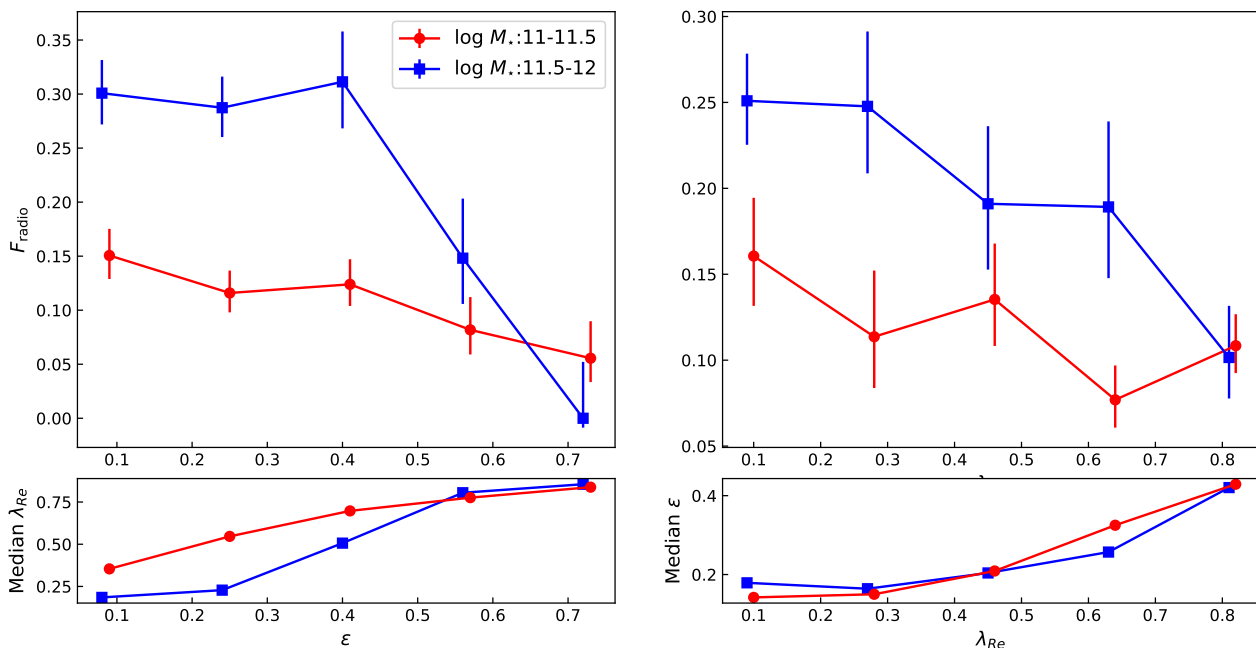
**Fig. 5.** $F_{\mathrm{radio}}$ for galaxies with different morphologies and kinematics. Top: $F_{\mathrm{radio}}$ as a function of $\epsilon$ and $\lambda_{R_e}$ for galaxies with different $M_\star$. The red dots and blue squares represent galaxies with $\log(M_\star/M_\odot) = 11 - 11.5$ and $11.5 - 12$, respectively. Bottom: Median $\lambda_{R_e}$ for galaxies in each $\epsilon$ bin and the median $\epsilon$ in each $\lambda_{R_e}$ bin. The red lines were shifted horizontally a bit for clarity.

son for this difference is that the three works use different sample criteria. Both Barišić et al. (2019) and Zheng et al. (2020) used mass-limited quiescent (non-star-forming) galaxy samples in their analyses, while Zheng et al. (2020) used radio AGNs with a much lower luminosity limit than Barišić et al. (2019). In our work, to enlarge the sample size, we included as many sources as possible regardless of $M_\star$ limits, colours, or radio luminosity limits. Therefore, the $F_{\mathrm{radio}}$-$\epsilon$ relation in this work is not, or only partially, in line with previous works.

In the top-right panel of Figure 5, the $F_{\mathrm{radio}}$ of high-$M_\star$ galaxies decreases monotonically with $\lambda_{R_e}$. For low-$M_\star$ galaxies, the $F_{\mathrm{radio}}$-$\lambda_{R_e}$ relation also shows a weak, decreasing trend despite small fluctuations. Based on these results, we conclude that radio AGNs are triggered more easily in galaxies with stronger random stellar motions (i.e. galaxies that have weaker stellar disc components).

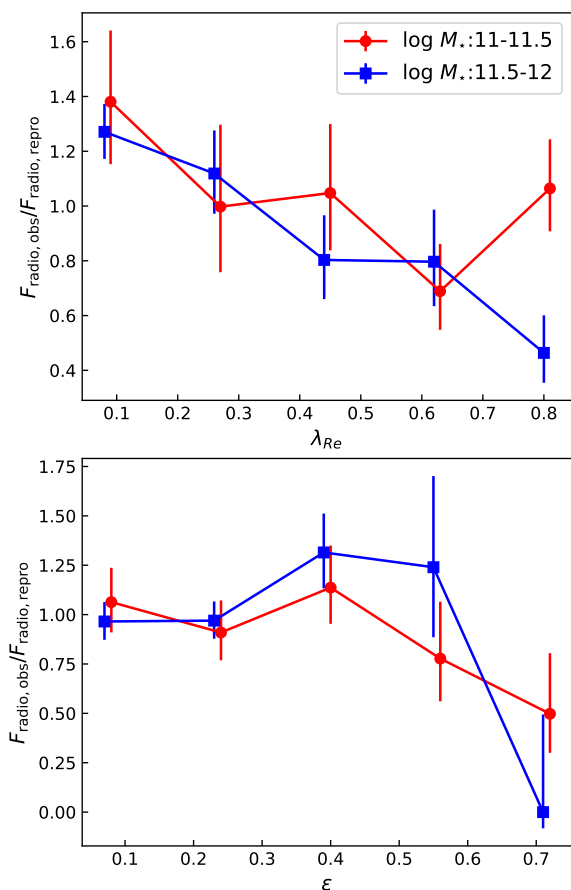### 3.3. Observed vs. reproduced $F_{\mathrm{radio}}$ relations

In the previous section, we show that $F_{\mathrm{radio}}$ is anti-correlated with both $\epsilon$ and $\lambda_{R_e}$. However, the morphologies and kinematics of galaxies are related to each other. For FRs, as shown in Figure 3, a large $\epsilon$ typically indicates the presence of a prominent disc component and a large $\lambda_{R_e}$ (see Eqs. 14-18 in Cappellari 2016). Above a characteristic mass of about $2 \times 10^{11} M_\odot$, galaxies start to be dominated by SRs, which have been assembled through dry mergers (see review Cappellari 2016, Sec. 7). The kinematics of SRs tend to be dominated by random motions. They do not have stellar discs and intrinsically have $\epsilon \lesssim 0.4$ in projection. Therefore, when plotting the median $\lambda_{R_e}$ or $\epsilon$ in each bin of Figure 5 as a function of the other parameter in the bottom panels of Figure 5, we observed clear increasing trends. These trends imply that the two $F_{\mathrm{radio}}$ relations actually reflect the same intrinsic link between jet-triggering probability and galaxy structure or evolu-

tionary path. In this section, we discuss which parameter is the better proxy of the intrinsic $F_{\mathrm{radio}}$ relation.

Because the two $F_{\mathrm{radio}}$ relations are connected by the correlation of $\epsilon$ and $\lambda_{R_e}$, one of the $F_{\mathrm{radio}}$ relations may be reproduced by the other. We first assumed that $\epsilon$ is a better predictor of $F_{\mathrm{radio}}$, and we expected that the $F_{\mathrm{radio}}$-$\lambda_{R_e}$ relations could be reproduced by the $F_{\mathrm{radio}}$-$\epsilon$ relation. We interpolated the observed $F_{\mathrm{radio}}$-$\epsilon$ relation to obtain a continuous function $\hat{F}_{\mathrm{radio}}(\epsilon)$. This function served as input as the 'intrinsic' probability of a galaxy with $\epsilon$ hosting a radio AGN. Next, we obtained the expected radio-loud probabilities for galaxies in each $\lambda_{R_e}$ bin based on their $\epsilon$ and $\hat{F}_{\mathrm{radio}}(\epsilon)$. The average of these expected probabilities was taken as the $\epsilon$-reproduced fraction of radio AGNs $F_{\mathrm{radio,repro}}$ in the corresponding $\lambda_{R_e}$ bin. We changed the role of $\epsilon$ and $\lambda_{R_e}$ in order to obtain the $\lambda_{R_e}$-reproduced $F_{\mathrm{radio}}$ in each $\epsilon$ bin. We present the ratio between the observed fraction of radio AGNs $F_{\mathrm{radio,obs}}$ and $F_{\mathrm{radio,repro}}$ in Figure 6.

If any of the $F_{\mathrm{radio}}$ relations can be predicted by the other $F_{\mathrm{radio}}$ relation and the $\epsilon$-$\lambda_{R_e}$ relation, we expected that the reproduced $F_{\mathrm{radio}}$ would be close to the observed value, and the decreasing trend in the $F_{\mathrm{radio}}$ relation would disappear in the $F_{\mathrm{radio}}$ ratio diagrams. In the top panel of Figure 6, the $F_{\mathrm{radio}}$ ratio $F_{\mathrm{radio,obs}}/F_{\mathrm{radio,repro}}$ for the high-$M_\star$ sample still shows a decreasing trend with $\lambda_{R_e}$. This means that the $F_{\mathrm{radio}}$-$\epsilon$ relation cannot reproduce the $F_{\mathrm{radio}}$-$\lambda_{R_e}$ relation. Therefore, $\epsilon$ is not sufficient for showing the intrinsic link between $F_{\mathrm{radio}}$ and galaxy structure. In contrast, the $F_{\mathrm{radio,obs}}/F_{\mathrm{radio,repro}}$-$\lambda_{R_e}$ relation for the low-$M_\star$ sample (top panel of Figure 6) and the $F_{\mathrm{radio,obs}}/F_{\mathrm{radio,repro}}$-$\epsilon$ relation for both samples (bottom panel of Figure 6) do not simply decline. This implies that $\lambda_{R_e}$ might be a good proxy for the intrinsic link between $F_{\mathrm{radio}}$ and galaxy structure in both samples. In the low-$M_\star$ sample, $\epsilon$ might also be used as a proxy, but it would be less robust than $\lambda_{R_e}$.

We note that the binning of data may weaken the significance of the analysis, and therefore we also compared the observed

These results show that the $F_{\mathrm{radio}}$ -$\lambda_{R_e}$ relation describes the intrinsic links between radio jets and host galaxies better than the $F_{\mathrm{radio}}$ -$\epsilon$ relation. Because $\lambda_{R_e}$ is a better proxy of the stellar kinematics of galaxies, this implies the triggering of radio AGNs is related to galaxy kinematics and assembly history. Furthermore, the $F_{\mathrm{radio}}$ -$\lambda_{R_e}$ and $F_{\mathrm{radio}}$ -$\epsilon$ relations should reveal the same underlying relation between radio AGNs and host galaxies because the $F_{\mathrm{radio}}$ -$\epsilon$ relation can be reproduced by the $F_{\mathrm{radio}}$ -$\lambda_{R_e}$ relations. However, $\epsilon$ is more easily affected by the inclination of galaxies, and this should explain the inability of the $F_{\mathrm{radio}}$ -$\epsilon$ to predict the $F_{\mathrm{radio}}$ -$\lambda_{R_e}$ well.
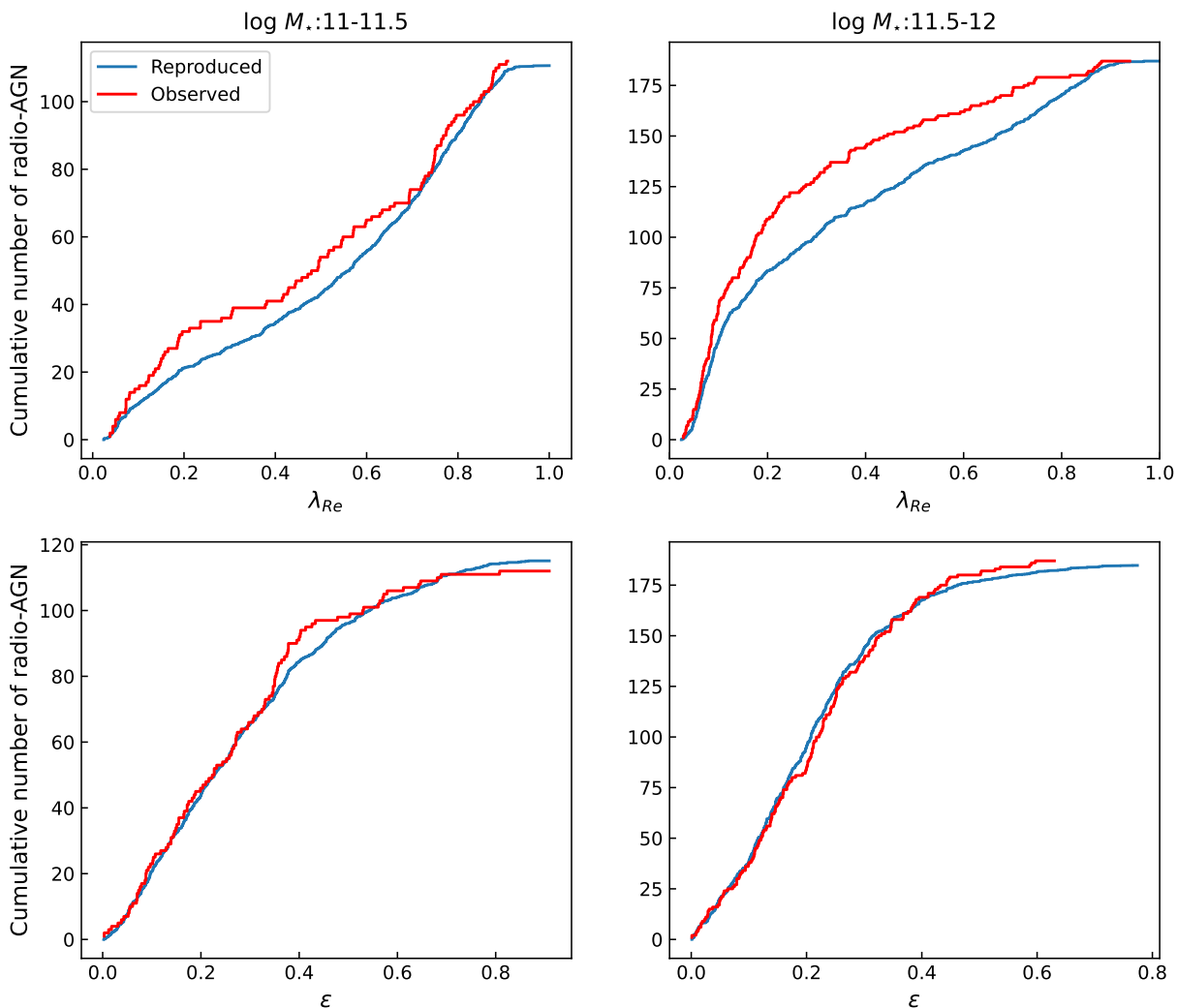
## 4. Conclusion and discussion

In this work, we combined the morphology and kinematic measurements for galaxies in the MaNGA survey with the data of radio AGNs from LoTSS DR2 and the NVSS-FIRST survey. We investigated the relations between radio AGNs and the kinematics of their host galaxies in $M_\star$ constrained samples. The main new findings in this article are briefly listed below:

– The radio luminosity of a radio AGN depends on the $\lambda_{R_e}$ of the host galaxy in our sample. Higher-luminosity radio AGNs could be hosted by galaxies with lower $\lambda_{R_e}$ at fixed $M_\star$.
– The fraction of galaxies hosting a radio AGN is higher in galaxies with smaller $\lambda_{R_e}$ in our sample. This trend is similar for both high- and low-$L_{150\,\mathrm{MHz}}$ radio AGNs.
– The $F_{\mathrm{radio}}$ -$\lambda_{R_e}$ relation cannot be well reproduced using the $F_{\mathrm{radio}}$ -$\epsilon$, while the $F_{\mathrm{radio}}$ -$\epsilon$ relation can be reproduced by the $F_{\mathrm{radio}}$ -$\lambda_{R_e}$ relation. This shows that the $F_{\mathrm{radio}}$ -$\lambda_{R_e}$ relation better describes the links between radio AGNs and host galaxies in our sample.

The dependence on $\lambda_{R_e}$ for radio AGNs in our work implies that the build-up history of galaxies could be related to the presence of radio jets. Because $\lambda_{R_e}$ quantifies the importance of the regular circular motion in a galaxy (in contrast to random motion), it is an indicator of the evolutionary path of the galaxy (Emsellem et al. 2007, 2011; Cappellari 2016). For galaxies built-up mainly from secular star forming processes, the ordered stellar motions are retained, and the stellar disc components are dominant in the galaxy structure; thus, the resulting $\lambda_{R_e}$ would not be very small. These galaxies are FRs. In contrast, SRs are likely to have a dry-major-merger dominated history, which would have led to the destruction of stellar discs and the enhancement of the random motions (i.e. a small $\lambda_{R_e}$). Therefore, the fact that high-$L_{150\,\mathrm{MHz}}$ radio AGNs favour small-$\lambda_{R_e}$ galaxies suggests that a merger history enhances the radio AGN activities.

We stress that this does not mean that all current high-luminosity radio AGNs are triggered directly by ongoing merger events, but a merger event in the past would make a galaxy become a breeding ground for powerful radio jets. The heritage of a merger event may influence a radio AGN's activity in at least two ways. Studies based on deep imaging (Tadhunter 2016; Pierce et al. 2019; Ramos Almeida et al. 2011) have shown that most of the galaxies with a radio-powerful AGN have past interaction signatures. The existence of these signatures may enhance gas inflow in the galaxy, facilitating fuelling of the central SMBH. However, this may not be the only reason for the $L_{150\,\mathrm{MHz}}$ -$\lambda_{R_e}$ dependence because secular processes may also form structures that benefit the gas inflow and could be responsible for all radiative mode AGNs (see e.g. Heckman & Best 2014; Sellwood 2014, for more details). Another consequence of a major merger

**Fig. 6.** Ratio of the observed and reproduced $F_{\mathrm{radio}}$. Top: $F_{\mathrm{radio}}$ ratio as a function of $\lambda_{R_e}$. The colours and symbols are similar to Figure 5. Bottom: $F_{\mathrm{radio}}$ ratio as a function of $\epsilon$. All red lines are shifted a bit horizontally.

and reproduced cumulative distribution of radio AGNs. The observed cumulative distribution of radio AGNs as a function of parameter $\theta$ ($\epsilon$ or $\lambda_{R_e}$) $Cum(\theta)$ is the number of radio AGNs with $\theta_i$ less than a given value as below:

$$Cum(\theta) = \sum_{i}^{N_{\mathrm{AGN}}} H(\theta - \theta_i), \tag{3}$$

where $H(x)$ is the Heaviside step function and the summation is for all radio AGNs. The reproduced cumulative distribution of radio AGNs as a function of $\lambda_{R_e}$ using $\hat{F}_{\mathrm{radio}}(\epsilon)$ can be calculated as

$$Cum_{\mathrm{repro}}(\lambda_{R_e}) = \sum_{i}^{N_{\mathrm{gal}}} \hat{F}_{\mathrm{radio}}(\epsilon_i) H(\lambda_{R_e} - \lambda_{R_e,i}), \tag{4}$$

where the summation is over all galaxies in the sample. Similarly, $Cum_{\mathrm{repro}}(\epsilon)$ can be obtained using $\hat{F}_{\mathrm{radio}}(\lambda_{R_e})$.

The cumulative distributions of radio AGNs for the two $M_\star$ groups are shown in Figure 7. The reproductions of the cumulative distributions clearly have different levels of goodness. For $Cum(\lambda_{R_e})$, the distributions reproduced from $\hat{F}_{\mathrm{radio}}(\epsilon)$ are significantly different from the observed distributions. On the contrary, the reproduced cumulative distributions $Cum_{\mathrm{repro}}(\epsilon)$ based on $\hat{F}_{\mathrm{radio}}(\lambda_{R_e})$ fit the observed distributions well.

**Fig. 7.** Cumulative distributions of radio AGNs. Top: Comparisons between the observed cumulative distributions of radio AGNs as a function of $\lambda_{R_e}$ and the $\epsilon$-reproduced distributions. Bottom: Comparisons between the observed cumulative distributions of radio AGNs as a function of $\epsilon$ and the $\lambda_{R_e}$-reproduced distributions.

event is the impact on the black hole spin. As mentioned in Section 1, it was suggested that a major merger could be an efficient way to make a high-spin black hole (Wilson & Colbert 1995; Moderski & Sikora 1996; Sikora et al. 2007; Fanidakis et al. 2011; Barišić et al. 2019) because the orbital angular momentum of the two progenitor SMBHs would transfer to the spin of the merged black hole. However, this theory might not be fully correct. Numerical simulations have shown that SMBHs reach their highest spin through coherent accretion processes at high redshifts when they have enough gas supply, and the merging of SMBHs at low redshifts would decrease the spin (Dubois et al. 2014; Bustamante & Springel 2019). The observational data also indicate that massive SMBHs might rotate more slowly than low-mass SMBHs(Reynolds 2013). These results would suggest that mergers do not enhance jet-launching processes by making a high-spin SMBH. It is more likely that mergers change the direction of the spin of SMBHs and influence the probability of launching a radio jet. Garofalo et al. (2010, 2020) indicated that radio jets are more powerful in counter-rotating disc systems, which can only exist in post-merger black holes. A counter-rotating disc system can also help form a magnetically arrested

disc, which is crucial for launching a powerful jet(Tchekhovskoy & McKinney 2012; Sikora & Begelman 2013; Rusinek et al. 2020). Therefore, we suggest that mergers can lead to a change in the black hole spin direction and boost the probability of producing a powerful jet. As a result, small-$\lambda_{R_e}$ galaxies (or SRs) can launch a powerful jet more easily than large-$\lambda_{R_e}$ galaxies (or FRs).

The $F_{\text{radio}}$-$\epsilon$ relation shows an overall decreasing trend but with a plateau at the small-$\epsilon$ part. We note that this trend is not fully consistent with previous research on the axis ratio of galaxies (Barišić et al. 2019; Zheng et al. 2020). A possible reason for this disparity is the difference in selection criteria of these works. Previous works were limited to colour-selected quiescent galaxies, which would exclude a large fraction of discy galaxies. This limitation causes large uncertainties in the $F_{\text{radio}}$ results for the large-$\epsilon$ (small-$q$) galaxies. However, the sample studied in this work is mainly composed of passive galaxies, and the $F_{\text{radio}}$-$\epsilon$ relation in this work does not change significantly when only the passive galaxies are included. The $M_\star$ limit adopted in the sample selection of Barišić et al. (2019) and Zheng et al. (2020) may also be a reason for our different results.

The link between the evolutionary path of galaxies and the presence of radio jets might also be related to the environment. First, environment richness is correlated with many important properties of galaxies. Galaxies in clusters tend to be more massive and are more likely to be elliptical galaxies than those in the field (see Blanton & Moustakas 2009; Conselice 2014, and references therein). Slow rotators also favour high density environments (Cappellari et al. 2011b). Second, the environment is connected to the prevalence and power of radio jets. Galaxies in cluster environments have a higher probability to be radio-loud than galaxies with a similar stellar mass in the field (Best et al. 2005a, 2007; Sabater et al. 2013). Radio AGNs also tend to have higher luminosity in higher density environments (Donoso et al. 2009; Croston et al. 2019). These results and the correlations between radio AGNs and galaxy kinematics in our work can be understood within the same scenario. We suggest the environmental trend of radio AGNs might be a result of the correlation between radio AGNs and galaxy kinematics. Galaxies in higher density environments are more likely to have a merger-dominant evolutionary history; thus, they are also more likely to be SRs, or low-$\lambda_{R_e}$ galaxies (Cappellari et al. 2011b; Cappellari 2016). Based on the results in our work, it is therefore not surprising that we can find more high-power radio AGNs in higher density environments.

Our work shows the potential of IFS surveys for studying the radio AGN-triggering mechanism. To better understand the link between radio AGNs and galaxy kinematics, it will be important to increase the sample in the next generation of IFS surveys. It will also be helpful to study the gas kinematics in these radio galaxies with deeper observations, which may provide important insights on the fuelling of the SMBHs.

# References

Abazajian, K. N., Adelman-McCarthy, J. K., Agüeros, M. A., et al. 2009, ApJS, 182, 543
Agresti, A. & Coull, B. A. 1998, The American Statistician, 52, 119
Ahumada, R., Prieto, C. A., Almeida, A., et al. 2020, ApJS, 249, 3
Baldwin, J. A., Phillips, M. M., & Terlevich, R. 1981, PASP, 93, 5
Balick, B. & Heckman, T. M. 1982, ARA&A, 20, 431
Barišić, I., van der Wel, A., van Houdt, J., et al. 2019, ApJ, 872, L12
Becker, R. H., White, R. L., & Helfand, D. J. 1995, ApJ, 450, 559
Bender, R., Burstein, D., & Faber, S. M. 1992, ApJ, 399, 462
Best, P. N. & Heckman, T. M. 2012, MNRAS, 421, 1569
Best, P. N., Kaiser, C. R., Heckman, T. M., & Kauffmann, G. 2006, MNRAS, 368, L67
Best, P. N., Kauffmann, G., Heckman, T. M., et al. 2005a, MNRAS, 362, 25
Best, P. N., Kauffmann, G., Heckman, T. M., & Ivezić, Ž. 2005b, MNRAS, 362, 9
Best, P. N., von der Linden, A., Kauffmann, G., Heckman, T. M., & Kaiser, C. R. 2007, MNRAS, 379, 894
Bevacqua, D., Cappellari, M., & Pellegrini, S. 2022, MNRAS, 511, 139
Binney, J. 1985, MNRAS, 212, 767
Blandford, R. D. & Znajek, R. L. 1977, MNRAS, 179, 433
Blanton, M. R. & Moustakas, J. 2009, ARA&A, 47, 159
Bois, M., Emsellem, E., Bournaud, F., et al. 2011, MNRAS, 416, 1654

Brown, M. J. I., Jannuzi, B. T., Floyd, D. J. E., & Mould, J. R. 2011, ApJ, 731, L41
Bundy, K., Bershady, M. A., Law, D. R., et al. 2015, ApJ, 798, 7
Bustamante, S. & Springel, V. 2019, MNRAS, 490, 4133
Cappellari, M. 2013, ApJ, 778, L2
Cappellari, M. 2016, ARA&A, 54, 597
Cappellari, M., Emsellem, E., Bacon, R., et al. 2007, MNRAS, 379, 418
Cappellari, M., Emsellem, E., Krajnović, D., et al. 2011a, MNRAS, 413, 813
Cappellari, M., Emsellem, E., Krajnović, D., et al. 2011b, MNRAS, 416, 1680
Cattaneo, A., Faber, S. M., Binney, J., et al. 2009, Nature, 460, 213
Chang, Y.-Y., van der Wel, A., da Cunha, E., & Rix, H.-W. 2015, ApJS, 219, 8
Chang, Y.-Y., van der Wel, A., Rix, H.-W., et al. 2013, ApJ, 773, 149
Chen, Y., Gu, Q., Fan, J., et al. 2021, ApJ, 913, 93
Condon, J. J., Cotton, W. D., & Broderick, J. J. 2002, AJ, 124, 675
Condon, J. J. & Dressel, L. L. 1978, ApJ, 221, 456
Conselice, C. J. 2014, ARA&A, 52, 291
Croston, J. H., Hardcastle, M. J., Mingo, B., et al. 2019, A&A, 622, A10
Donoso, E., Best, P. N., & Kauffmann, G. 2009, MNRAS, 392, 617
Dubois, Y., Volonteri, M., Silk, J., Devriendt, J., & Slyz, A. 2014, MNRAS, 440, 2333
Dunn, R. J. H. & Fabian, A. C. 2006, MNRAS, 373, 959
Emsellem, E., Cappellari, M., Krajnović, D., et al. 2011, MNRAS, 414, 888
Emsellem, E., Cappellari, M., Krajnović, D., et al. 2007, MNRAS, 379, 401
Fabian, A. C. 2012, ARA&A, 50, 455
Fanidakis, N., Baugh, C. M., Benson, A. J., et al. 2011, MNRAS, 410, 53
Garofalo, D., Evans, D. A., & Sambruna, R. M. 2010, MNRAS, 406, 975
Garofalo, D., North, M., Belga, L., & Waddell, K. 2020, ApJ, 890, 144
Graham, M. T., Cappellari, M., Bershady, M. A., & Drory, N. 2019, arXiv e-prints, arXiv:1910.05139
Graham, M. T., Cappellari, M., Li, H., et al. 2018, MNRAS, 477, 4711
Heckman, T. M. & Best, P. N. 2014, ARA&A, 52, 589
Lauer, T. R. 2012, ApJ, 759, 64
Law, D. R., Cherinka, B., Yan, R., et al. 2016, AJ, 152, 83
McNamara, B. R. & Nulsen, P. E. J. 2007, ARA&A, 45, 117
Moderski, R. & Sikora, M. 1996, A&AS, 120, 591
Mulcahey, C. R., Leslie, S. K., Jackson, T. M., et al. 2022, arXiv e-prints, arXiv:2206.01195
Pierce, J. C. S., Tadhunter, C. N., Ramos Almeida, C., Bessiere, P. S., & Rose, M. 2019, MNRAS, 487, 5490
Ramos Almeida, C., Tadhunter, C. N., Inskip, K. J., et al. 2011, MNRAS, 410, 1550
Reynolds, C. S. 2013, Classical and Quantum Gravity, 30, 244004
Rusinek, K., Sikora, M., Kozieł-Wierzbowska, D., & Gupta, M. 2020, ApJ, 900, 125
Sabater, J., Best, P. N., & Argudo-Fernández, M. 2013, MNRAS, 430, 638
Sabater, J., Best, P. N., Hardcastle, M. J., et al. 2019, A&A, 622, A17
Sánchez, S. F., Kennicutt, R. C., Gil de Paz, A., et al. 2012, A&A, 538, A8
Sayeb, M., Blecha, L., Kelley, L. Z., et al. 2021, MNRAS, 501, 2531
Sellwood, J. A. 2014, Reviews of Modern Physics, 86, 1
Shimwell, T. W., Tasse, C., Hardcastle, M. J., et al. 2019, A&A, 622, A1
Sikora, M. & Begelman, M. C. 2013, ApJ, 764, L24
Sikora, M., Stawarz, Ł., & Lasota, J.-P. 2007, ApJ, 658, 815
Smee, S. A., Gunn, J. E., Uomoto, A., et al. 2013, AJ, 146, 32
Smith, E. P., Heckman, T. M., & Illingworth, G. D. 1990, ApJ, 356, 399
Stoughton, C., Lupton, R. H., Bernardi, M., et al. 2002, AJ, 123, 485
Tadhunter, C. 2016, A&A Rev., 24, 10
Tchekhovskoy, A. & McKinney, J. C. 2012, MNRAS, 423, L55
van der Wel, A., Rix, H.-W., Holden, B. P., Bell, E. F., & Robaina, A. R. 2009, ApJ, 706, L120
van Haarlem, M. P., Wise, M. W., Gunst, A. W., et al. 2013, A&A, 556, A2
Wake, D. A., Bundy, K., Diamond-Stanic, A. M., et al. 2017, AJ, 154, 86
Wang, J., Kong, M.-Z., Liu, S.-F., et al. 2019, Research in Astronomy and Astrophysics, 19, 144
Wang, J., Xu, Y., Xu, D. W., & Wei, J. Y. 2016, ApJ, 833, L2
Wilson, A. S. & Colbert, E. J. M. 1995, ApJ, 438, 62
Wright, E. L., Eisenhardt, P. R. M., Mainzer, A. K., et al. 2010, AJ, 140, 1868
York, D. G., Adelman, J., Anderson, John E., J., et al. 2000, AJ, 120, 1579
Zheng, X. C., Röttgering, H. J. A., Best, P. N., et al. 2020, A&A, 644, A12
Zheng, X. C., Röttgering, H. J. A., van der Wel, A., & Duncan, K. 2022, A&A, 665, A114